scales of the disk correspond to those of the large-scale radio jets and lobes. For example, the kinetic timescale in which the radio jet structures change is about 10^6 yr, while the synchrotron lifetimes of radio regions range from $\sim 10^6$ yr for the hot spots to $\sim 10^8$ yr for the more extended lobes. Similarly, the total 'equipartition' energy in the lobes, $\sim 10^{57}$ erg, corresponds to the mass energy available in the disk: for a dust/gas ratio similar to our Galaxy, the disk mass is about 10^5 solar masses. Converted to energy at an efficiency of 1%, a value often assumed, this mass would yield 10^{57} erg.

These facts, combined with the alignment of the radio axis and disk spin axis, lead us to describe the feature seen in NGC4261 as the 'outer accretion disk' of the central active nucleus. The bright unresolved point at the centre of the disk probably represents thermal optical emission from the hot inner accretion disk. The outer disk supplies fuel by way of the inner disk to the central engine, probably a massive black hole, in quantities that determine the luminosity, size and orientation of the extended radio emission.

Hints of such features have been obtained earlier: a previous ground-based image of NGC4261 showed a small central dust region ($\sim 3''$ in diameter), but neither its size nor morphology could be accurately determined. Molecular radio observations[12] of Centaurus A have indicated the presence of rotating cold material in a rather larger region (~ 1 kpc). To our knowledge, however, the image presented here is the first of an accretion disk where size and structure can be directly associated with the results of nuclear activity.

On much larger scales, dust has been seen before in many other elliptical galaxies[9,13], as lanes, disks and filamentary structures. These structures, often assumed to be the remnants of a captured late-type galaxy, are generally 10 to 100 times larger than the disk shown here. Although their presence may be correlated statistically with nuclear activity, their dynamic and decay timescales are much longer than those associated with AGN phenomena.

If the disk is in simple circular rotation, measurements of the rotation curve at HST resolution should lead to an estimate of the central mass that is free from the ambiguities of estimates derived from the orbits of stars. Measurements of the turbulent velocities should help to constrain models of the nature of the angular momentum and mass transport in the disk[11]. □

Received January; accepted May 1993.

1. Rees, M. J. *A. Rev. Astr. Astrophys.* **22**, 471–506 (1984).
2. Baade, D. & Lucy, L. B. *Messenger* **61**, 24–27 (1990).
3. Peletier, R. F., Davies, R. L., Illingworth, G. D., Davis, L. E. & Cawson, M. *Astr. J.* **100**, 1091–1142 (1989).
4. Davies, R. L. & Birkinshaw, M. *Astrophys. J.* **303**, L45–49 (1986).
5. Jacoby, G. H., Ciardullo, R., Ford, H. C. *Astrophys.J.* **356**, 332–349 (1990).
6. de Vaucouleurs, G. *Astrophys.J. suppl. Series* **6**, 213–234 (1961).
7. Binggeli, B., Sandage, A. & Tammann, G. A. *Astr.J.* **90**, 1681-1758 (1985).
8. Mollenhóff, C., Bender, R. *Astr. Astrophys.* **174**, 63–66 (1987).
9. Kormendy, J., Stauffer, J. in *IAU Symp. No. 127, 'Structure and Dynamics of Elliptical Galaxies'* (ed. de Zeeuw, P. T.) 405–406 (Reidel, Dordrecht, 1987).
10. Birkinshaw, M. & Davies, R. C. *Astrophys.J.* **291**, 32–44 (1985).
11. Pringle, J. E. *A. Rev. Astr. Astrophys.* **19**, 137–162 (1981).
12. Israel, F. P. *et al. Astr. Astrophys.* **227**, 342–350 (1990).
13. Bertola, F. in *IAU Symp. No. 127, 'Structure and Dynamics of Elliptical Galaxies'* (ed. de Zeeuw P. T.) 135–143 (Reidel, Dordrecht, 1987).

Century-scale effects of increased atmospheric CO_2 on the ocean–atmosphere system

Syukuro Manabe & Ronald J. Stouffer

Geophysical Fluid Dynamics Laboratory/NOAA Princeton University, PO Box 308, Princeton, New Jersey 08542, USA

SEVERAL studies have addressed the likely effects of CO_2-induced climate change over the coming decades [1–10], but the longer-term effects have received less attention. Yet these effects could be very significant, as persistent increases in global mean temperatures may ultimately influence the large-scale processes in the coupled ocean–atmosphere system that are thought to play a central part in determining global climate. The thermohaline circulation is one such process — Broecker has argued[11] that it may have undergone abrupt changes in response to rising temperatures and ice-sheet melting at the end of the last glacial period. Here we use a coupled ocean–atmosphere climate model to study the evolution of the world's climate over the next few centuries, driven by doubling and quadrupling of the concentration of atmospheric CO_2. We find that the global mean surface air temperature increases by about 3.5 and 7 °C, respectively, over 500 years, and that sea-level rise owing to thermal expansion alone is about 1 and 2 m respectively (ice-sheet melting could make these values much larger). The thermal and dynamical structure of the oceans changes markedly in the quadrupled-CO_2 climate — in particular, the ocean settles into a new stable state in which the thermohaline circulation has ceased entirely and the thermocline deepens substantially. These changes prevent the ventilation of the deep ocean and could have a profound impact on the carbon cycle and biogeochemistry of the coupled system.

The model used here[8] consists of a general circulation model (GCM) of the atmosphere and oceans, and a simple model of land surfaces that includes the budgets of heat and water. It is a global model with realistic geography. The atmospheric GCM includes the seasonal variation of insolation, and predicted cloud over which depends only on the relative humidity. It has nine vertical finite difference levels. The horizontal distribution of predicted variables is represented by spherical harmonics (15 associated Legendre functions for each of 15 Fourier components) and by corresponding grid-point values. The oceanic GCM uses a finite difference technique with a regular grid system which has horizontal spacing (4.5° latitude) by (3.75° longitude) and 12 vertical levels. This model is similar to that of Bryan and Lewis[12], except that it mimics the effect of mesoscale eddies by the diffusion of potential temperature and salinity on isopycnal surfaces. The atmospheric and oceanic GCMs interact through the exchange of heat, water and momentum.

Assuming the temporal variations of atmospheric CO_2 in Fig. 1*a*, three 500-year integrations of the coupled model are done. One is a standard integration (S) in which the atmospheric CO_2 remains unchanged. In a second integration (4×C), the CO_2 concentration increases by 1% yr^{-1} (compound) (close to the 'business as usual' (BAU) radiative forcing rate obtained by the Intergovernmental Panel on Climate Change[13]; IPCC) until it reaches four times the normal value at about the 140th year and remains unchanged thereafter. In a third integration (2×C), the CO_2 concentration also increases at the rate of 1% yr^{-1} (compound) until it doubles around the 70th year and remains unchanged thereafter. By comparing the three integrations, one can evaluate the long-term impact of the doubling and quadrupling of atmospheric CO_2 on the coupled system.

The initial conditions for these integrations have realistic seasonal and geographical distributions of surface temperature, surface salinity and sea ice; the atmospheric and oceanic components of the model are nearly in equilibrium with these distributions. When the time integration of the model starts from this initial condition, the model climate rapidly drifts towards its own equilibrium state. To minimize the drift, the fluxes of heat and water at the ocean–atmosphere interface are adjusted by amounts that vary seasonally and geographically[8]. These adjustments, applied to all three integrations identified above, are independent of the anomalies of temperature and

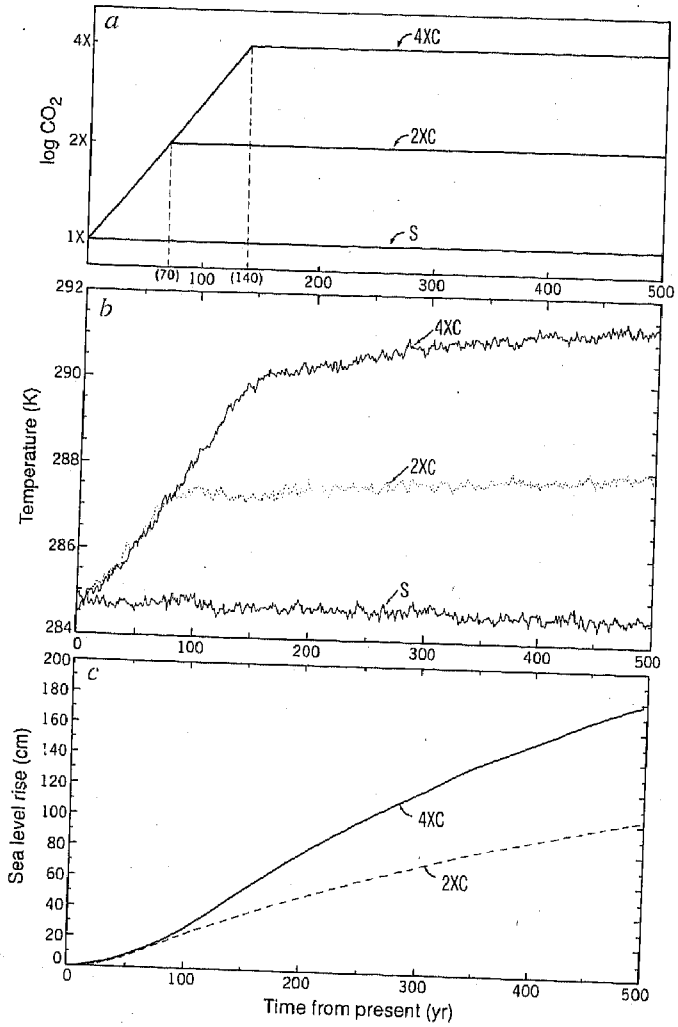

FIG. 1 Temporal variations of: *a*, logarithm of atmospheric CO_2 concentration; *b*, global mean surface air temperature (K); and *c*, global mean increase of sea level (cm) due to thermal expansion, computed as the difference between 4×C and S, and 2×C and S.

salinity at oceanic surface, and so neither damp nor amplify the anomalies.

Figure 1*b* contains the time series of global mean surface air temperature from the 4×C, 2×C, and S integrations. During the first 140 years of the 4×C integration, the global mean surface air temperature increases by 5 °C, at the rate of ~3.5 °C per century. After the 140th year, the global mean surface air temperature increases slowly by an additional 1.5 °C despite the absence of further CO_2 increase in the model atmosphere. The large thermal inertia of the deep ocean is mainly responsible for this residual warming.

A qualitatively similar feature is evident in the time series of the 2×C integration. During the first 70 years, the global mean temperature increases by 2.2 °C, again at the rate of 3.5 °C per century. After atmospheric CO_2 stops increasing at the 70th year, the global mean surface air temperature increases by an additional 1 °C.

The temporal variations of global mean sea level due to thermal expansion of sea water alone are estimated for both the 4×C and 2×C integrations (Fig. 1*c*), although sea level is not explicitly predicted in the present model[12]. During the first few decades of the 4×C experiment, the sea level rises by ~1 cm per decade. The sea level continues to rise long after the 140th year when the atmospheric carbon dioxide stops increasing. A qualitatively similar feature is indicated in the curve of sea-level rise in the 2×C integration. The total sea-level rise over the entire 500-year period of the 4×C amounts to about 1.8 m and is substantially larger than the corresponding rise of about 1 m in the 2×C.

Although the melt water from continental ice sheets is not included in the computation of sea-level rise mentioned above, the rate of melting at the surface of ice sheets has been estimated from the surface heat budget. If the effect of melt water were taken into consideration, the resulting sea-level rise could be much larger.

Figure 2 indicates that, in the 4×C, the thermohaline circulation (THC) almost disappears in most of the model oceans, leaving behind wide-driven cells. For example, the THC nearly vanishes in the North Atlantic during the first 200-yr integration (Fig. 3). In the immediate vicinity of the Antarctic continent, the THC weakens and becomes shallower (Fig. 2), markedly reducing the formation of Antarctic Bottom Water. This in turn weakens the northward flow of bottom water in both Pacific and Atlantic.

The near-extinction of the THC described above is attributable mainly to the capping of oceans by relatively fresh water in high latitudes, where the supply of water to the ocean surface increases markedly. The excess of precipitation over evaporation and runoff from continents increases in high-latitude oceans because of the enhanced poleward transport of water vapour in the warmer model troposphere.

The evolution of the THC in 4×C described above can be

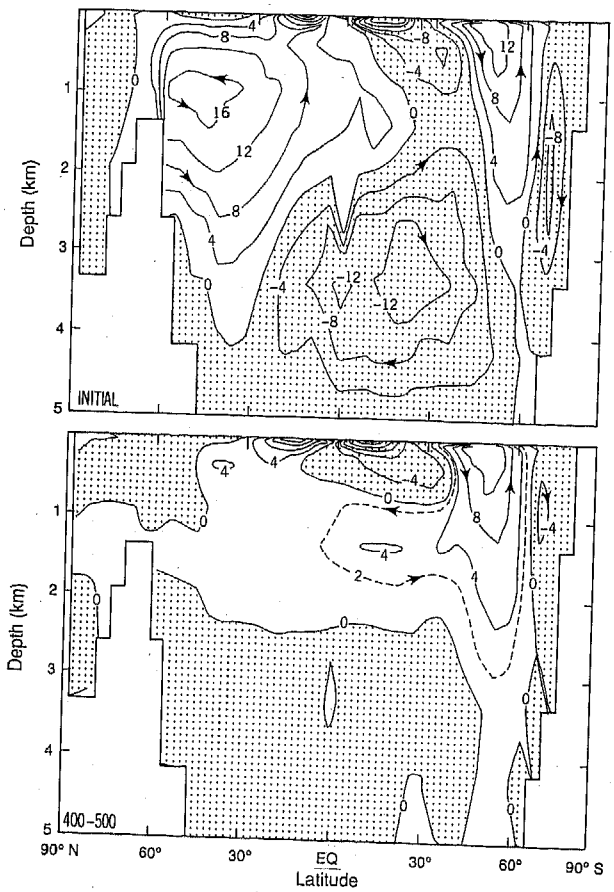

FIG. 2 Stream function of zonal mean meridional circulation in model oceans. Top: initial distribution obtained from the S. Bottom: average over the 400–500th year of the 4×C. Units on contours are in Sverdrups (10^6 m^3 s^{-1}).

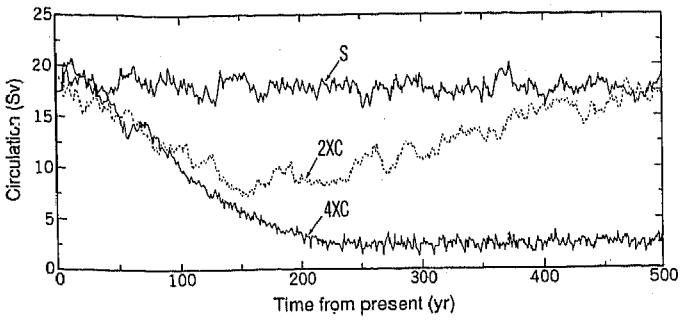

FIG. 3 Temporal variation of the intensity of the thermohaline circulation in the North Atlantic from the 4×C, 2×C and S. Here the intensity is defined as the maximum value of the stream function representing the meridional circulation (for example Fig. 2) in the North Atlantic.

compared with the 2×C in which the atmospheric carbon dioxide increases until it doubles (Fig. 3). In the 2×C, the intensity of the THC in North Atlantic again keeps decreasing long after the 70th year when atmospheric CO_2 stops increasing and the rates of surface warming and freshening are abruptly reduced; it is eventually reduced to less than half of its original intensity. The THC begins to recover very slowly, however, around the 150th year of the integration. Because of the reduction of the upward advection of cold water that accompanies the weakening of the THC, a large warming of the subsurface layer takes place in the 2×C between the Equator and 45° N latitude in the North Atlantic. The resulting increase in the density contrast between the sinking and rising regions seems to be responsible for the gradual recovery of the THC in the North Atlantic by the 500th year.

The results from the 2×C described above imply that the weakening of the THC in the Atlantic during the early phases of both experiments does not represent the collapse of the circulation due to an instability. Instead, it represents a slow adjustment to the evolving density structure of the model Atlantic Ocean. Once the THC vanishes in the 4×C integration, however, it does not regenerate despite the intensification and deep penetration of positive temperature anomaly in low and middle latitudes. This suggests that the state of inactive THC reached in the 4×C is a stable state which is distinct from the state of the active circulation maintained in the early phase of both integrations. The existence of two stable equilibria in a coupled ocean–atmosphere model has been demonstrated previously[14].

It is important to recognize that an adjustment of surface water flux is needed to sustain the THC in the Atlantic Ocean of the present model[14]. Although the adjustments of heat and water fluxes are independent of the anomalies of the sea surface temperature and salinity, and do not affect the damping rate of these anomalies, the sensitivity of the THC in the present coupled model could be significantly different from the actual sensitivity. Therefore, even if atmospheric carbon dioxide is quadrupled, the near-disappearance of the THC may not occur in the real ocean. On the other hand, if the freshening of near-surface water due to the melting of continental ice sheets had been incorporated into the model, it could have induced the disappearance of the THC in the 2×C.

Towards the end of the 4×C experiment, the thermocline becomes deeper, particularly over the North Atlantic, where the near-disappearance of thermohaline circulation results in significant warming and increased salinity of intermediate water. The rise of surface air temperature (Fig. 4) is particularly large (11–16 °C) over the Arctic Ocean where sea ice disappears almost completely during the warmer half of the year by the end of the CO_2-quadrupling integration. On the other hand, it is smaller (5–8 °C) in the northern North Atlantic and the Circumpolar Ocean of the Southern Hemisphere. Here the increase of sea surface temperature is reduced because of vertical mixing of heat in the oceans[8]. The warming over continents ranges from 7 °C to 10 °C and is larger than that over oceanic regions with the exception of the Arctic Ocean mentioned above. The temperature change described above is almost as large as the difference between the present climate and the warm climate of the Late Cretaceous[15] approximately 65–90 million years ago. In the 2×C, the pattern of surface air temperature resembles, but is half as large as, the change in 4×C.

Averaged globally, the rate of increase in surface air temperature is ~3.5 °C per century during the first 150 years of the 4×C when the atmospheric concentration of carbon dioxide increases at the rate of 1% yr^{-1} (roughly the BAU rate obtained by the IPCC). This is slightly larger than the IPCC's best estimate of 3.0 °C per century. It has been estimated that the equilibrium response of the present model to the doubling of atmospheric CO_2 is approximately 3.5 °C in global mean surface air temperature. This response belongs in the upper half of the 1.5–4.5 °C range of climate sensitivity estimated by the IPCC. Thus, it is possible that the present model may exaggerate the sensitivity of the actual climate.

According to the IPCC, a quadrupling of the CO_2 equivalent of greenhouse gases could be realized if the BAU emission of greenhouse gases continued until the end of the twenty-first century. Draconian measures would probably be required to prevent the CO_2 equivalent of greenhouse gases from quadrupling[16]. Considering the possible overestimate of climate sensitivity by the present model, it may be reasonable to speculate that the 2×C and 4×C experiments provide a probable range of future climate change. Nevertheless, one should not discard too readily the possibility of very large long-term climate change such as that which occurred in the 4×C experiment.

Received 4 May 1993; accepted 27 May 1993.

1. Bryan, K., Komro, F. G., Manabe, S. & Spelman, M. J. *Science* **215**, 56–58 (1982).
2. Schlesinger, M. E., Gates, W. L. & Han, Y. J. *Coupled Ocean–Atmosphere Models* (ed.

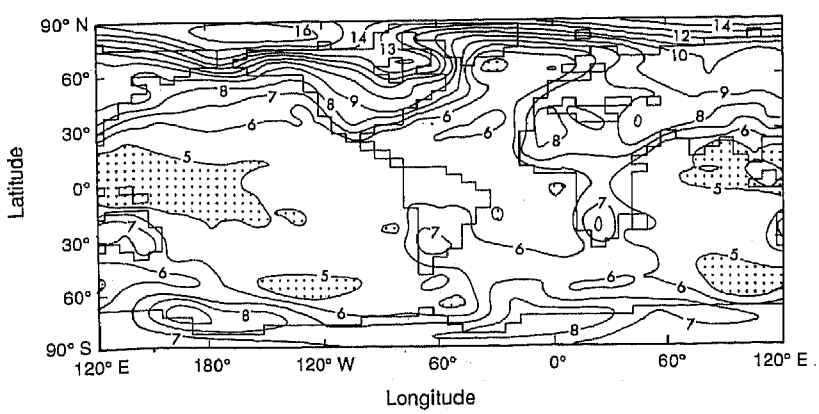

FIG. 4 Geographical distributions of the increase of surface air temperature from the CO_2-quadrupling experiment computed as the difference between the time mean values over the 400–500th year of the 4×C and the S integrations.

Nihoul, J. C. J.) 447–478 (Elsevier, 1985).
3. Bryan, K. & Spelman, M. J. *J. geophys. Res.* **909**(C6), 11679–11688 (1985).
4. Bryan, K., Manabe, S. & Spelman, M. J. *J. phys. Oceanogr.* **18**, 851–867 (1988).
5. Washington, W. M. & Meehl, G. A. *Clim. Dynamics* **4**, 1–38 (1989).
6. Stouffer, R. J., Manabe, S. & Bryan, K. *Nature* **342**, 660–662 (1989).
7. Manabe, S., Bryan, K. Spelman, M. J. *J. phys. Oceanogr.* **20**, 772–749 (1990).
8. Manabe, S., Stouffer, R. J., Spelman, M. J. & Bryan, K. *J. Clim.* **4**, 785–818 (1991).
9. Hansen, J. *et al. J geophys. Res.* **93**, 9341–9864 (1988).
10. Cubasch, U. *et al. Clim. Dynamics* **8**, 55–69 (1992).
11. Broecker, W. S. *Nature* **328**, 123–126 (1987).
12. Bryan, K. & Lewis, L. J. *J. geophys. Res.* **84**, 2503–2517 (1979).
13. Intergovernmental Panel on Climate Change *Scientific Assessment of Climate*, WMO-UNEP (Cambridge Univ. Press, 1990).
14. Manabe, S. & Stouffer, R. J. *J. Clim.* **1**, 841–866 (1988).
15. Crowly, T. J. & North, G. N. *Paleoclimatology. Oxford Monogr. Geol. Geophys.* **16**, (1991).
16. Walker, J. C. G. & Kasting, J. F. *Paleogeogr. Paleoclimatol. Paleoecol.* **97**, 151–189 (1992).

ACKNOWLEDGEMENTS. We thank K. Dixon for his advice on model improvements and J. D. Mahlman, K. Bryan and T. R. Toggweiler for their comments on the paper.

Evidence for general instability of past climate from a 250-kyr ice-core record

W. Dansgaard*, S. J. Johnsen* †, H. B. Clausen*, D. Dahl-Jensen* N. S. Gundestrup*, C. U. Hammer*, C. S. Hvidberg*, J. P. Steffensen*, A. E. Sveinbjörnsdottir †, J. Jouzel ‡ & G. Bond §

* The Niels Bohr Institute, Department of Geophysics, University of Copenhagen, Haraldsgade 6, DK-2200 Copenhagen N, Denmark
† Science Institute, Department of Geophysics, University of Iceland, Dunhaga 3, IS-107, Reykjavik, Iceland
‡ Laboratoire de Modélisation du Climat et de l'Environment, CEA/DSM, CE Saclay 91191, and Laboratoire de Glaciologie et Géophysique de l'Environment, BP 96, 38402 St Martin d'Héres Cedex, France
§ Lamont-Doherty Geological Observatory, Columbia University, Palisades, New York 10964, USA

RECENT results[1,2] from two ice cores drilled in central Greenland have revealed large, abrupt climate changes of at least regional extent during the late stages of the last glaciation, suggesting that climate in the North Atlantic region is able to reorganize itself rapidly, perhaps even within a few decades. Here we present a detailed stable-isotope record for the full length of the Greenland Ice-core Project Summit ice core, extending over the past 250 kyr according to a calculated timescale. We find that climate instability was not confined to the last glaciation, but appears also to have been marked during the last interglacial (as explored more fully in a companion paper[3]) and during the previous Saale–Holstein glacial cycle. This is in contrast with the extreme stability of the Holocene, suggesting that recent climate stability may be the exception rather than the rule. The last interglacial seems to have lasted longer than is implied by the deep-sea SPECMAP record[4], in agreement with other land-based observations[5,6]. We suggest that climate instability in the early part of the last interglacial may have delayed the melting of the Saalean ice sheets in America and Eurasia, perhaps accounting for this discrepancy.

In 1990–92, the joint European Greenland Ice-core Project (GRIP) drilled an ice core to near the bedrock at the very top of the Greenland ice sheet (72.58° N, 37.64° W; 3,238 m above sea level[7]; annual mean air temperature −32 °C). The 3,028.8-m-long core was recovered by an electromechanical drill, ISTUK[8]. Less than 1 m of core in total was lost in the drilling process. The deepest 6 m is composed of silty ice with pebbles. The core quality is excellent, except for a 'brittle zone' in the depth interval between 800 and 1,300 m.

Here we discuss a timescale for the entire core and present a continuous profile of $\delta^{18}O$ (hereafter denoted by δ, the relative deviation of the $^{18}O/^{16}O$ ratio in a sample from that in standard mean ocean water). In polar glacier ice, δ is mainly determined by its temperature of formation[9]. Profiles of several climate-related parameters spanning the last interglacial period (known as the Eemian period, or Eem) are being investigated by GRIP participants[3].

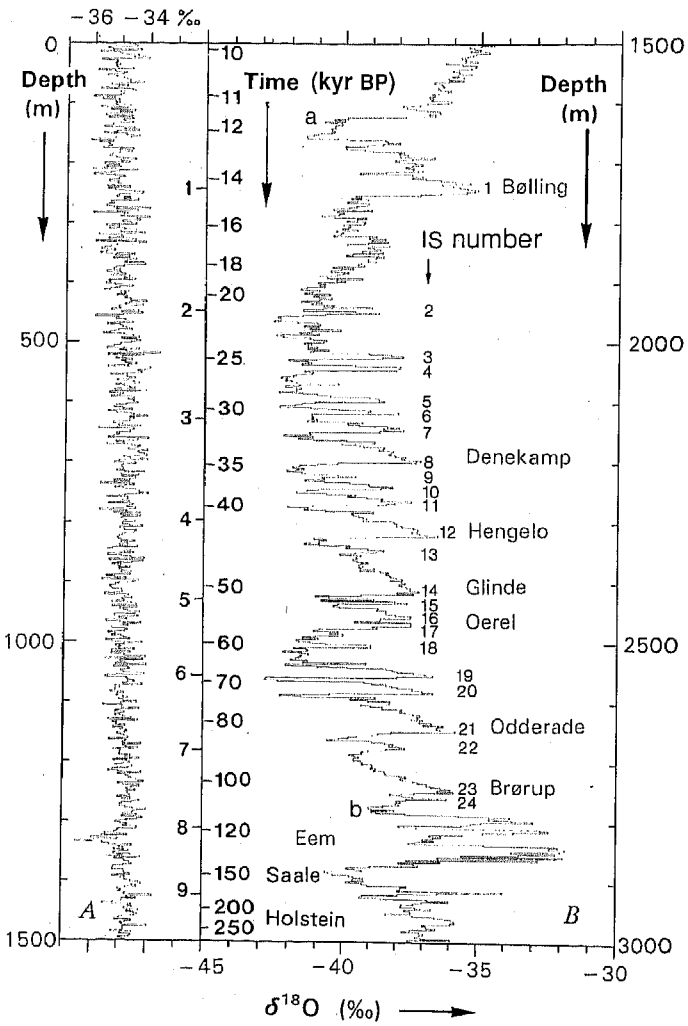

FIG. 1 The continuous GRIP Summit $\delta^{18}O$ record plotted in two sections on a linear depth scale: *A*, from surface to 1,500 m; *B*, from 1,500 to 3,000 m depth. Each point represents 2.2 m of core increment. Glacial interstadials are numbered to the right of the *B* curve. The timescale in the middle is obtained by counting annual layers back to 14.5 kyr BP, and beyond that by ice flow modelling. The glacial insterstadials of longest duration are reconciled with European pollen horizons[16].

The timescale back to 14.5 kyr BP (thousands of years before present) is derived by counting annual layers downward from